(Proposal to Jefferson Lab PAC 32)

Scaling Study of the L-T Separated Pion Electroproduction Cross Section at 11 GeV

June 20, 2007

P. Bosted, H. Fenker, D. Gaskell, T. Horn[1] (co-spokesperson), M. Jones, D. Mack
G.R. Smith, M. Spata, S. Wood
Jefferson Lab, Newport News, Virginia

C. Butuceanu, G.M. Huber (co-spokesperson), G.J. Lolos, Z. Papandreou
University of Regina, Regina, Canada

W. Boeglin, P. Markowitz
Florida International University, Miami, Florida

A. Asaturyan, A. Mkrtchyan, H. Mkrtchyan, V. Tadevosyan
Yerevan Physics Institute, Yerevan, Armenia

E. Brash
Christopher Newport University, Newport News, Virginia

C.F. Perdrisat
College of William and Mary, Williamsburg, Virginia

K. Aniol
California State University Los Angeles, Los Angeles, California

E. Christy, C.E. Keppel, L. Tang, V. Tvaskis
Hampton University, Hampton, Virginia

D. Hornidge
Mount Allison University, Sackville, Canada

A. Sarty
Saint Mary's University, Halifax, Canada

V. Punjabi
Norfolk State University, Norfolk, Virginia

J. Calarco
University of New Hampshire

[1] Contact person: hornt@jlab.org

Abstract

The purpose of this experiment is to measure the Q^2 dependence of the longitudinal and transverse cross sections for the exclusive $\mathrm{p}(e, e'\pi^+)\mathrm{n}$ reaction above the resonance region at fixed values of x_B=0.31, 0.40, and 0.50 and $-t$. The Q^2 dependence of the longitudinal cross section will provide a test of whether the data have, or are evolving towards the Q^{-6} scaling prediction for hard exclusive processes for $\mathrm{Q}^2 \leq 10$ GeV^2.

The extraction of Generalized Parton Distributions from hard exclusive reactions relies on the dominance of the longitudinal component, while transverse contributions are assumed to be negligible. However, recent results from Jefferson Lab suggest that σ_T may be relatively large in the kinematically accessible regime. The goal of this measurement is to provide a high quality, systematic data set of separated longitudinal and transverse π^+ cross sections, which may place a constraint on the value of Q^2 for which one can reliably apply perturbative QCD concepts and extract Generalized Parton Distributions.

The data might also allow for further theoretical studies to identify elements that may be missing from calculations in charged vector meson production and constrain possible longitudinal backgrounds in the extraction of the pion form factor.

I. CONTRIBUTION TO THE HALL C 12 GEV UPGRADE

Garth Huber intends to apply to the Natural Sciences and Engineering Research Council of Canada (NSERC) for a Research Tools and Instrumentation grant (approximately $100kUSD) in support of the SHMS Heavy Gas Čerenkov detector. Given the currently-projected CD2 and CD3 review schedule, this application will likely be submitted in October, 2008. Should these funds be granted by the Government of Canada, he intends to lead the construction efforts of this detector in collaboration with Hall C scientific and technical staff. In either event, the Regina group intends to provide manpower in support of the R&D, construction and commissioning of this detector.

Tanja Horn is supporting the SHMS optics design. She is working on the evaluation of the radiative heating of the SHMS horizontal bender magnet. This entails in part creating and maintaining a simulation of the magnet and the analysis of data obtained with a prototype. In addition, she is working with the design and engineering division on the implementation of spectrometer optics calculations to guide the design and construction of the SHMS, and in particular, the horizontal bender.

II. SCIENTIFIC BACKGROUND

A. Introduction

By performing a measurement of separated p$(e, e'\pi^+)$n cross sections to test the factorization of long-distance from short-distance physics in hard exclusive processes, we have the unique opportunity to lay the foundation for a reliable interpretation of results from one of the highest priority 12 GeV programs at Jefferson Lab, the extraction of Generalized Parton Distributions (GPDs). This measurement is of particular interest for our understanding of hadronic structure in terms of quark gluon degrees of freedom in the transition region from the hadronic to the partonic regime for Q^2 up to 10 GeV^2. The extraction of GPDs from pion electroproduction data relies on the dominance of the longitudinal cross section, and the proposed experiments typically assume that the contribution of transversely polarized photons is negligible. However, recent experimental results [1] suggest that the transverse contribution of the cross section is still relatively large at Q^2=2.45 GeV^2, which, if also true at higher values of Q^2, would limit the interpretability of the data in terms of GPDs.

Before considering the extraction of GPDs from pion electroproduction data, it is necessary to demonstrate that Q^2 scaling applies in the JLab 12 GeV kinematic regime. Although there is no single criterion for the applicabiliy of factorization, tests of every necessary condition can provide evidence for having reached the Q^2 scaling regime. In particular, we must confirm that $\sigma_L \gg \sigma_T$ as expected from GPD models. This requires measurements of both longitudinal and transverse components, and thus high precision L/T separations.

The goal of this proposal is to test the dominance of the longitudinal cross section in charged pion electroproduction by making a systematic measurement of the Q^2 dependence of the π^+ longitudinal and transverse cross sections. In the asymptotic limit one expects that the longitudinal cross section evolves towards Q^{-6} scaling, while transverse contributions are suppressed by an additional factor of Q^{-2}. This is different from the simple pion pole exchange picture, where σ_L changes more rapidly than σ_T as Q^2 and t_{min} increases, reflecting the decreasing influence of the pion pole. A significant longitudinal response may be indicative of the realization of the scaling expectation of the GPD formalism for charged pion electroproduction.

The results from this measurement may also help to identify missing elements in existing calculations of the pion production cross section, which will help to constrain longitudinal backgrounds in the extraction of the pion form factor from pion electroproduction data.

We propose to measure forward π^+ electroproduction by detecting the produced pion in coincidence with the scattered electron using the Hall C SHMS+HMS configuration. We will extract the separated longitudinal and transverse cross sections via the Rosenbluth separation technique. Measurements in non-parallel kinematics will allow for simultaneous extraction of the interference terms and tests of the $-t$ dependence of the π^+ cross section.

B. Partons and Factorization

The conventional picture of the hadron, in which partons play the dominant role, predicts a separation of short-distance and long-distance physics. The separation scale is given by the four-momentum transfer squared (Q^2). Earlier measurements of inclusive processes such as deep-inelastic scattering (DIS) confirm that in the limit of large Q^2, at fixed values of the Bjorken variable x_B, such processes can be viewed as scattering from individual partons within the hadronic system. A similar separation (factorization) of scales may be expected to apply to hard exclusive scattering and allow for using perturbative QCD (pQCD) concepts in the description of hadrons.

In recent years, much progress has been made to develop a comprehensive framework for describing the quark-gluon structure of the nucleon based on the concept of Generalized Parton Distributions (GPDs). GPDs unify the momentum-space parton densities in inclusive deep-inelastic scattering with the spatial densities (e.g., hadronic form factors) measured in elastic scattering. The main difference between the regular parton distribution functions (PDFs) and the GPDs is that the latter include correlations between different parton configurations. While PDFs represent the probability to find a parton with a particular polarization and longitudinal momentum fraction x_B, the GPDs represent the interference of wavefunctions, one where the parton has a momentum fraction of $x_B + \xi$ and one where this fraction is $x_B - \xi$, where ξ is the longitudinal component of the momentum transfer to the nucleon.

In order to access the physics contained in the GPDs, one is limited to the hard scattering regime. A universal and important feature of hard exclusive reactions is that one can separate perturbative and non-perturbative stages of the interaction. This is known as the hard/soft "factorization" property. The presence of a hard probe allows for the creation of small size quark-antiquark and gluon configurations whose interactions are described by pQCD concepts. The non-perturbative part of the reaction describes how the hadron reacts to this configuration, or how the probe is transformed into hadrons. This separation of the interaction is the "factorization" of hard reactions.

A factorization theorem has been proven for longitudinally polarized photons, which correspond to small size configurations of quarks and gluons, in meson electroproduction [2]. It states that for sufficiently large values of Q^2, at fixed x_B, and fixed momentum transfer to the nucleon, $-t$, the amplitude for hard exclusive reactions can be expressed in terms of a hard process, a distribution amplitude describing the formation of the final state meson, and Generalized Parton Distributions (GPDs), which encode the non-perturbative physics inside the nucleon. This is known as the "handbag" diagram (see Figure 1). Note that a single hard gluon is exchanged in the hard subprocess, in which a virtual photon couples to a single quark inside the nucleon. Though it is expected that the factorization theorem is valid for $Q^2 \geq 10$ GeV^2, to date it is unclear whether it may already be applicable at moderately high values of Q^2 under certain conditions [3].

One of the predictions of the factorization theorem is that in the limit of large Q^2, the

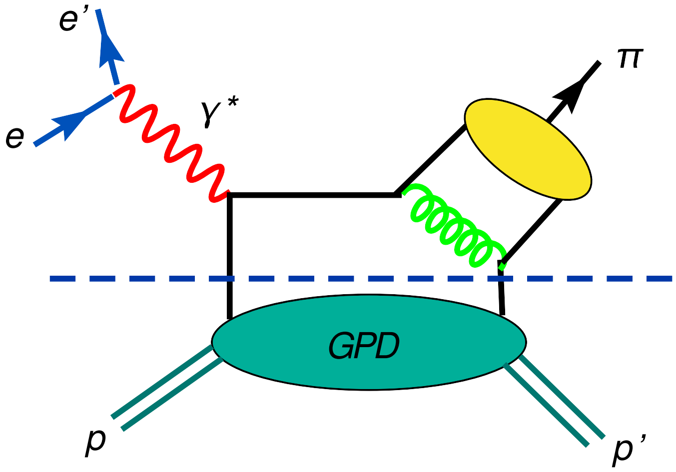

FIG. 1: *Diagram of the factorization theorem for longitudinally polarized photons in meson electroproduction. For sufficiently large values of Q^2, at fixed x_B and fixed momentum transfer to the nucleon $-t$, the amplitude for hard exclusive reactions can be expressed in terms of a hard process, a distribution amplitude describing the formation of the final state meson, and Generalized Parton Distributions (GPDs), which encode the non-perturbative physics inside the nucleon. This is known as the "handbag" diagram.*

dominant virtual photon polarization is longitudinal. The corresponding cross section scales to leading order like $\sigma_L \sim Q^{-6}$ at fixed x_B and $-t$, modulo higher order corrections. The contribution of transversely polarized photons is suppressed by an additional power of $1/Q$ in the amplitude. In the Q^2-scaling limit, pQCD describes the short distance process and GPDs provide access to the non-perturbative physics. The dominance of the longitudinal contribution by a factor of $1/Q$ is important because it contains the GPDs one would in fact like to extract. GPDs are universal objects that describe the structure of the nucleon in a process-independent way, and combine the characteristics of parton distributions with those of elastic form factors. At leading order, the information on the nucleon structure can be parameterized in terms of four quark chirality conserving GPDs, denoted by H, E, $\tilde{H}$, and $\tilde{E}$. The GPDs H and E are summed over the quark helicity, and $\tilde{H}$ and $\tilde{E}$ include the difference between right and left handed quarks. H and $\tilde{H}$ conserve the proton helicity, while E and $\tilde{E}$ allow for proton helicity flip. Since the quark helicity must be conserved in the hard scattering regime, the electroproduced meson acts as a helicity filter. Leading order QCD predicts that meson production is sensitive only to the unpolarized GPDs, H and E, while in the case of π^+ production the amplitudes involve only the axial GPDs, $\tilde{H}$ and $\tilde{E}$, whose first moments can be related to the axial and pseudoscalar form factors [4].

$$\int_{-1}^{1} dx \tilde{H}(x;t) = G_A(t),$$
$$\int_{-1}^{1} dx \tilde{E}(x;t) = G_P(t). \tag{1}$$

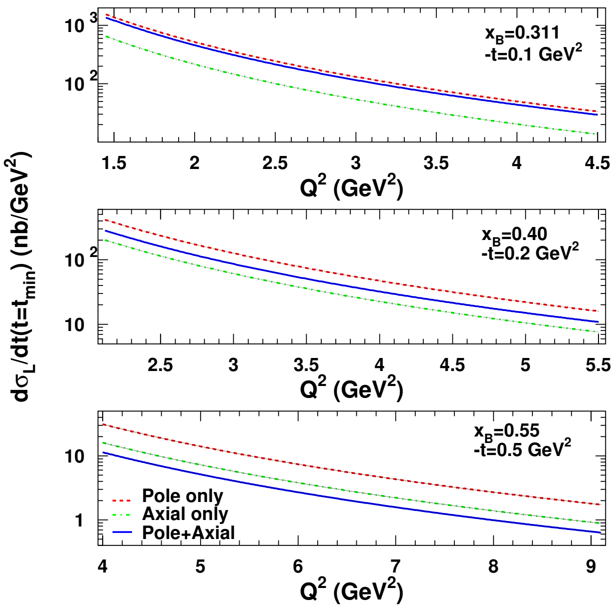

FIG. 2: *The π^+ production cross section at fixed values of x_B and $-t$. The pion pole and axial contributions, as predicted by a GPD calculation [7], are represented by the red dashed and the green dashed-dotted lines respectively.*

The pion production amplitude for a virtual photon can be written (schematically) [5],

$$M_\pi^L \sim (A_{\pi N} + B_{\pi N}). \tag{2}$$

For π^+ production, the amplitudes A and B are given by [3, 6],

$$\begin{aligned} A_{\pi^+ p} &\sim (\tilde{H}^u - \tilde{H}^d)(e_u + e_d), \\ B_{\pi^+ p} &\sim (\tilde{E}^u - \tilde{E}^d)(e_u + e_d). \end{aligned} \tag{3}$$

In the limit $-t \to m_\pi^2$, the π^+ production amplitude contains an additional pion pole contribution, which appears as a strong singularity in the function $\tilde{E}^u - \tilde{E}^d$. $\tilde{E}$ is a particularly interesting quantity, as it cannot be related to the known parton distributions, and so could provide new information about nucleon structure that cannot be easily obtained from any other source.

Deeply virtual Compton scattering (DVCS) holds great promise for tests of the factorization theorem at moderate values of Q^2, where recent results from Hall A [8, 9] and Hall B [10] indicate consistency with the factorization prediction. However, since DVCS depends at the same time on both the unpolarized (H and E) and the polarized ($\tilde{H}$ and $\tilde{E}$) GPDs, only 2-3 of which may dominate in a given kinematic setting [11], tests of the individual components are quite challenging. The sensitivity to the quark-flavor dependence is, for instance, entirely eliminated. Thus, data from hard meson electroproduction provide additional information that is important for disentangling

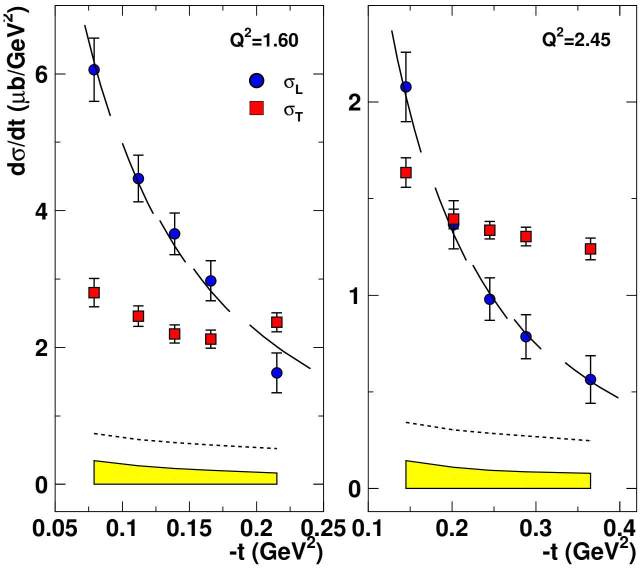

FIG. 3: *The $-t$ dependence of the longitudinal and transverse π^+ cross sections. The data points are from the recently completed analysis of the E01-004 (F_π-2) experiment [1].*

the different GPDs.

While DVCS depends on all four quark-flavor dependent GPDs, longitudinal meson electroproduction depends only on either a combination of the unpolarized or the polarized GPDs, and thus acts as a helicity filter. The $\tilde{H}$ and H components typically dominate DVCS, because E and $\tilde{E}$ are kinematically suppressed. However, H and $\tilde{H}$ contributions are also important in meson electroproduction. In the case of π^+ production, the presence of the t-channel pole results in the dominance of $\tilde{E}$ at small $-t$. In addition, it is difficult to raise $-t$ sufficiently to make $\tilde{E}$ and $\tilde{H}$ comparable without violating the Collins condition that $-t$ should be much smaller than Q^2.

As already discussed, the pion pole contribution is generally assumed to dominate the π^+ production amplitude at low $-t$. However, the leading order QCD calculation of Ref. [6] finds that the pion pole term is only about a factor of 3 larger than the non-pole term at x_B=0.30, indicating that $\tilde{H}$ may not be entirely overwhelmed by $\tilde{E}$ at these kinematics. This was also shown in the caclulations of Ref. [11]. At larger momentum transfers, the GPD model by Vanderhaeghen, Guidal and Guichon predicts a less favorable ratio, as indicated by the curves in Fig. 2. It is clearly important to improve our knowledge of these non-pole contributions, as they provide information about the longitudinal backgrounds entering in the extraction of the pion form factor from electroproduction experiment proposed for the JLab 12 GeV program [12]. Sufficiently precise measurements of the Q^2 dependence of σ_L at fixed x_B, or alternately, of the x_B dependence of σ_L at fixed Q^2, would be of significant value in constraining our knowledge of these non-pole contributions.

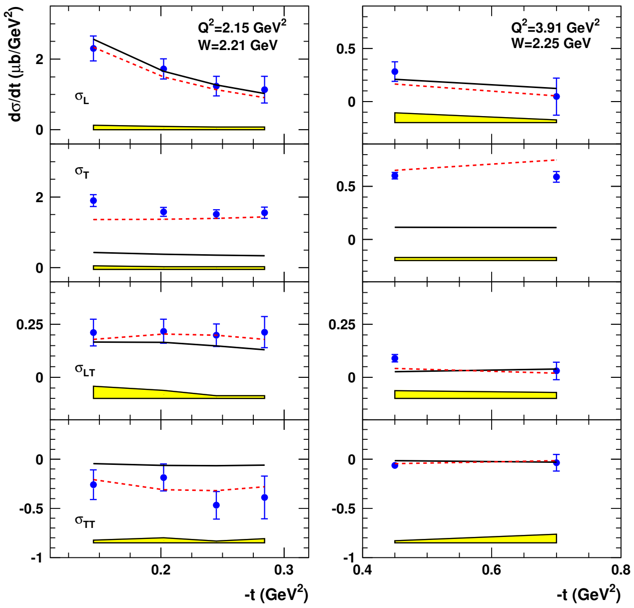

FIG. 4: *The $-t$-dependence of the separated cross sections from E01-107 data. The error bars include the statistical and uncorrelated systematic uncertainty combined in quadrature, and the error band includes the correlated and $-t$-correlated systematic uncertainties. The solid black lines denote the best fit of the VGL/Regge model [13] to the data. The fit parameter is the pion cutoff, which relates to the pion form factor in a monopole form. The red dashed curve denotes the cross section parameterization using previous JLab data that was used for the rate estimates in this proposal.*

The size of transverse contributions to the forward pion electroproduction cross section at moderate values of Q^2 has been controversial for a long time, and the lack of L-T separated data in this region complicates theoretical estimates. Figure 3 shows the results from experiment E01-004 (F_π-2), which suggest that the contribution of transversely polarized photons is still significant at Q^2=2.45 GeV^2 [1]. This trend is confirmed by the recently completed analysis of experiment E01-107 [14]. Figure 4 shows the results at Q^2=2.15 GeV^2 and Q^2=3.91 GeV^2. The relative contribution of σ_T is approximately a factor of two larger than that of σ_L. This trend may be expected since the pole dominated term, σ_L, decreases more rapidly with increasing distance from the pole, while σ_T is largely independent of it. However, it should be noted that a significant transverse contribution to the cross section complicates the extraction of GPDs from the leading order term, which is assumed to be dominated by σ_L. The large value of σ_T may indicate that the GPD picture is not yet applicable in this kinematic regime. Indeed, the DVCS data of Refs. [9, 15] are equally well described by a Regge pole exchange model with unitarity constraint [16]. Thus, there is a clear need for new data over a sufficiently broad kinematic range to allow the dominant reaction mechanisms at present and 12 GeV JLab energies to be better understood.

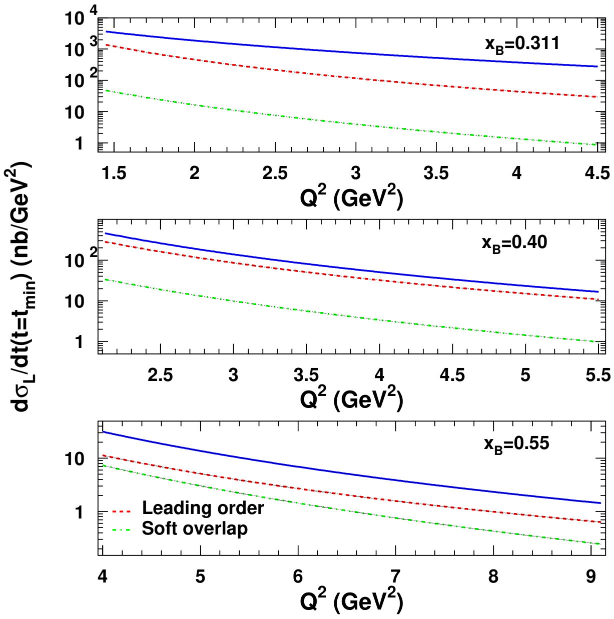

FIG. 5: *Longitudinal π^+ cross section at $-t$=$-t_{min}$ for the proposed kinematic range. The dashed line denotes the leading order result, the dashed-dotted line the soft overlap contribution, and the solid line shows the combined result as predicted by a GPD calculation from reference [7].*

C. Previous Data and Analysis

One of the most stringent and model independent tests for the characteristic signature of QCD factorization is the Q^2 power law scaling of the separated cross sections. The hard scattering predictions are $\sigma_L \sim Q^{-6}$ and $\sigma_T \sim Q^{-8}$. If the Q^2 dependence of the cross section is consistent with this prediction, the cross section data may be used to further constrain phenomenological models of GPDs. The Q^2 dependence of σ_T does, however, provide less conclusive evidence for having reached the hard scattering regime as the factorization theorem was proven rigorously only for longitudinal photons [2].

Higher order corrections play an important role at experimentally accessible energies [3, 5], and competing soft mechanisms may mimic the expected Q^2-scaling behavior characteristic for the hard pQCD term [17]. The contribution of power corrections to the leading order σ_L as predicted by the GPD model by Vanderhaeghen, Guichon and Guidal [11] is shown in Figure 5. At x_B=0.3, the soft overlap contribution is more than an order of magnitude below the leading order prediction. At larger x_B where approximations made in the calculations of the soft overlap are expected to be even more adequate [11], the soft overlap contributions are still about an order of magnitude below the hard amplitude. The soft overlap contribution drops approximately as Q^{-8}, which is the result expected at large Q^2.

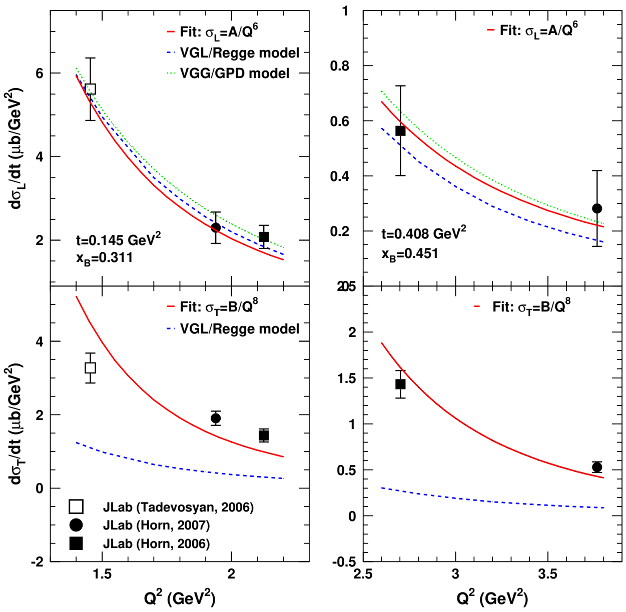

FIG. 6: *The Q^2-dependence of the separated cross sections at fixed values of $-t$ and x_B. The error bars denote statistical and systematic uncertainty combined in quadrature. The red, solid curve indicates a fit of the form Q^{-6} for σ_L, and Q^{-8} for σ_T. The green dotted line is a GPD calculation from reference [7]. In this calculation power corrections to the leading order are included. The blue dashed line is a VGL/Regge calculation using Λ_π^2 from a global fit to F_π.*

Previous exclusive meson electroproduction data above the resonance region are available from Jefferson Lab experiments such as Hall B experiment E99-105 [18] and Hall C experiments E93-021 [19, 20], E91-003 [21], E01-004 [1], and E01-107 [22]. One of the goals of the Hall B measurement was to access the GPDs through the x_B and $-t$ dependencies of exclusively electroproduced vector mesons. The experiment was carried out using the large acceptance CLAS detector. The differential cross section for meson production was measured in a kinematic region of W >2.0 GeV, covering Q^2 from 1.5 to 3.5 GeV^2 and momentum transfer $-t$ below 1.5 (GeV/c)^2. Though the extraction of the interference terms could be achieved using the CLAS acceptance, the measured cross sections could not always be separated into the components corresponding to longitudinally and transversely polarized photons without additional assumptions. The ρ^0 and ω cross sections show relatively good agreement with the Q^2 scaling prediction. However, considerable transverse contributions complicate the isolation of contributions from the handbag mechanism from these data [23, 24]. Additional information on the relative size of longitudinal and transverse components may therefore be of interest for further interpretation of these existing data.

The Q^2-dependence of the p$(e, e'\pi^+)$n longitudinal and transverse cross sections, where results from experiment E01-107 have been combined with recent results from Jefferson Lab Hall

C, is shown in Figure 6. While the scaling laws are reasonably consistent with the Q^2-dependence of the σ_L data, the two additional predictions, that $\sigma_L \gg \sigma_T$ and $\sigma_T \sim Q^{-8}$, are not consistent with the data.

D. Impact on Existing and Future GPD Measurements

The proposed π^+ electroproduction experiment above the resonance region is essential for a better understanding of both existing data [1, 19] and proposed 12 GeV measurements at Jefferson Lab [25]. The experimental longitudinal cross section data are generally well described by modern calculations based on Regge theory like the one by Vanderhaeghen, Guidal and Laget (VGL). However, the transverse contribution is significantly underpredicted by the VGL/Regge model up to values of Q^2=3.91 GeV^2. Though the magnitude of σ_T is better described by recent calculations treating the ρ meson exchange in a different way than in the VGL model [26], it fails to describe the existing σ_T data at higher Q^2. An improved calculation for σ_T, including additional mechanisms, is currently underway [16]. It will benefit from the results of this measurement, which may provide important information on the elements that are missing in the existing calculations. These data may also help to constrain longitudinal backgrounds in the extraction of the pion form factor.

The ratio of the σ_L and σ_T is of significant interest to the study of exclusive π^+ cross sections with CLAS12 at 12 GeV [25]. A large acceptance device like CLAS is well suited to map out the x_B, $-t$, and the Q^2 dependence of various processes to constrain GPD models as thoroughly as possible without the correlations between $-t$ and x_B characteristic of parallel kinematics. Depending on the relative size of σ_L and σ_T, a detailed study of the separated π^+ cross section using CLAS12 alone may be difficult. If σ_L is relatively small, absolute measurements of the separated cross sections may require additional information from a double-arm spectrometer setup like the one in Hall C. The maximum Q^2 value accessible for π^+ production in CLAS12 is about 10 GeV^2 for unseparated cross sections, which is well matched with the kinematics proposed for this measurement. Provided that meaningful L/T separations can be performed using CLAS12, the maximum Q^2 would be approximately 6 GeV^2 for separated cross sections.

The separated results from the proposed measurement may play an important part in guiding the 12 GeV GPD π^+ program. Indeed, recent studies of DVCS data have raised new questions about the accessibility of GPDs at JLab energies. There, the experience with inclusive deep-inelastic scattering (DIS) suggests that the leading-twist approximation should be applicable already at values of Q^2 as low as a few GeV^2, which seems to be consistent with the first results on the Q^2 dependence of DVCS observables. However, recent DVCS cross section results are also well described by the Regge pole exchange model with unitarity constraint. If charged pion electroproduction is going to be useful for testing models of GPDs at 12 GeV JLab energies, we expect to see evidence of soft-hard factorization or the approach to it. In particular, we must confirm that $\sigma_L \gg \sigma_T$. **If the transverse contribution to the cross section is larger than anticipated,**

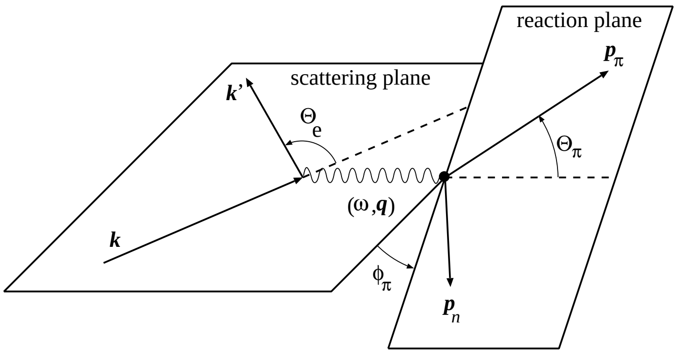

FIG. 7: *Kinematics of the $p(e, e'\pi^+)n$ reaction.*

this would dramatically influence the experimental kinematical accessibility of GPDs using charged pion electroproduction in 12 GeV experiments.

Previous data suggest that the ratio of σ_T/σ_L is about 0.5 for π^- production on the neutron [30]. In addition, the VGL Regge model, which is in relatively good agreement with these data, predicts that σ_T/σ_L continues to decrease as Q^2 increases. Indeed, if the transverse contributions to the cross section are suppressed, the σ_T/σ_L ratio in π^- production provides a way to extract σ_L in the n$(e, e'\pi^-)$p reaction from unseparated, high ϵ measurements without an explicit L/T separation. A determination of this ratio would thus greatly improve the ability of large acceptance devices like CLAS12 to study this reaction.

III. EXPERIMENTAL METHOD

In this experiment we will measure separated cross sections for the p$(e, e'\pi^+)$n reaction using the Rosenbluth separation technique. In addition, we will measure σ_T/σ_L for π^- production from the neutron.

The kinematics of the p$(e, e'\pi^+)$n reaction are illustrated in Figure 7. The incident electron with four momentum k=$(\epsilon_k$,$\mathbf{k})$ scatters through an angle θ_e to a final four momentum q=$(\omega$,$\mathbf{q})$. The electron scattering plane is defined by the three momenta $\mathbf{k}$ and $\mathbf{k}'$, and also includes the exchanged virtual photon three momentum transfer $\mathbf{q}$. The virtual photon is absorbed by the target proton and a pion is emitted with four-momentum p'=$(E(p'$,$\mathbf{p}))$, where $\mathbf{p}$ is oriented relative to the scattering plane by a polar angle θ_π and an azimuthal angle ϕ_π.

The unpolarized pion electroproduction cross section can be written as the product of a virtual photon flux factor and a virtual photon cross section,

$$\frac{d^5\sigma}{d\Omega_e dE'_e d\Omega_\pi} = J\left(t, \phi \rightarrow \Omega_\pi\right) \Gamma_v \frac{d^2\sigma}{dt d\phi}, \tag{4}$$

where $J\left(t, \phi \rightarrow \Omega_\pi\right)$ is the Jacobian of the transformation from $dtd\phi$ to $d\Omega_\pi$, ϕ is the azimuthal angle between the scattering and the reaction plane, and Γ_v=$\frac{\alpha}{2\pi^2}\frac{E'_e}{E_e}\frac{1}{Q^2}\frac{1}{1-\epsilon}\frac{W^2-M^2}{2M}$ is the virtual photon flux factor. The virtual photon cross section can be expressed in terms of contributions from transversely and longitudinally polarized photons,

$$2\pi\frac{d^2\sigma}{dtd\phi} = \frac{d\sigma_T}{dt} + \epsilon\frac{d\sigma_L}{dt} + \sqrt{2\epsilon(1+\epsilon)}\frac{d\sigma_{LT}}{dt}cos\phi + \epsilon\frac{d\sigma_{TT}}{dt}cos2\phi. \tag{5}$$

Here, $\epsilon = \left(1 + 2\frac{|\mathbf{q^2}|}{Q^2}\tan^2\frac{\theta}{2}\right)^{-1}$ is the virtual photon polarization, where $\mathbf{q^2}$ is the square of the three-momentum transferred to the nucleon and θ is the electron scattering angle. The interference terms, σ_{LT} and σ_{TT}, can be eliminated by averaging over ϕ_{pq}, and the longitudinal and transverse cross sections can be separated by measuring the cross section at two or more values of ϵ.

The equivalent π^- cross sections from the neutron will be obtained by taking both π^+ and π^- data on the deuteron. The π^- cross section will be extracted from,

$$\sigma_n^{\pi^-} = \sigma_D^{\pi^-}\frac{\sigma_p^{\pi^+}}{\sigma_D^{\pi^+}}. \tag{6}$$

The π^+ data on the deuteron is necessary to cancel possible wave function effects [27].

The virtual photon polarization is crucial in QCD factorization tests. In particular, QCD factorization applies strictly speaking only to longitudinal photons, which are expected to dominate at large Q^2. The amplitude for transversely polarized photons cannot be expressed in terms of GPDs. This is a result of longitudinal photons coupling, on average, to configurations of significantly smaller size than the transverse ones.

In parallel kinematics, it is not possible to measure the $-t$ dependence of the cross section, since W, Q^2, and $-t$ are not independent variables. In order to measure the $-t$ dependence one must vary θ_π away from parallel kinematics. In this case σ_{LT} and σ_{TT} also contribute and additional data are required for a complete ϕ_π coverage. The interference terms can then be obtained from the ϕ dependence of the data.

It is not always possible to vary Q^2 while keeping $-t$ and x_B constant. Figure 8 shows the accessible phase space. The kinematically forbidden region is separated by solutions corresponding to parallel kinematics. The region above $-t_{min}$ is accessible to large acceptance devices like the CLAS. However, note that due to the kinematically forbidden region the kinematic coverage is limited there as well. For example, at $-t$=0.3, a measurement with the CLAS would be limited to $x_B < 0.45$.

In meson electroproduction processes at experimentally accessible values of Q^2, there will always be non-negligible soft contributions from configurations of normal hadronic size [28]. These contributions are expected to become less important as Q^2 increases. Trying to describe these "higher twist" corrections in terms of QCD degrees of freedom may not always be the most feasible approach. One possibility for experiments designed to study GPDs and the transition to the partonic regime is to provide sufficient information for theoretical calculations to separate contributions from small-size and hadronic-size configurations. Precocious factorization holds great promise in accessing GPDs, as higher order corrections are expected to cancel in the asymmetries

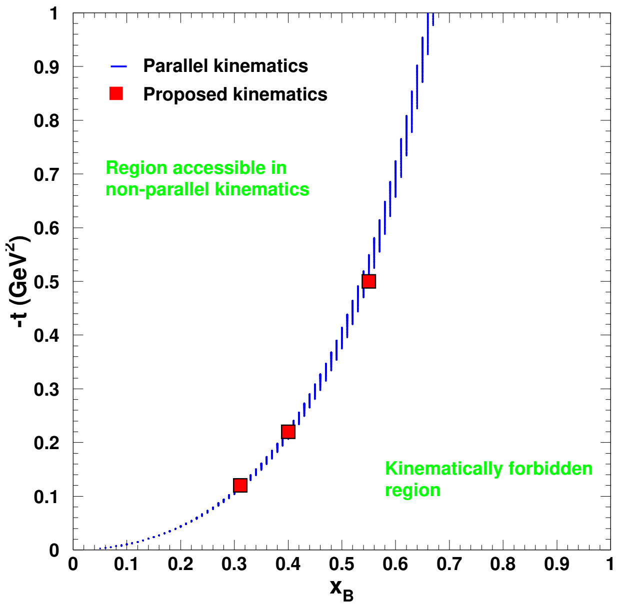

FIG. 8: *The $-t$ versus x_B phase space available for L-T separations in Hall C at 11 GeV using the SHMS+HMS combination. The blue lines correspond to parallel kinematics and suggest a strong correlation between $-t$ and x_B. The region above t_{min} corresponds to non-parallel kinematics and is accessible to large acceptance devices like the CLAS.*

or ratios of observables. However, the observation of Q^2 scaling in asymmetries or ratios of observables, while indicative of cancellation of higher order corrections, is not necessarily a stringent test of factorization itself. For example, transverse contributions in both the numerator and denominator may conspire to give the appearance of Q^2 scaling, but one would obtain the wrong size for the absolute asymmetry. A stricter test, in which higher order corrections are more likely to be apparent, are measurements of absolute cross sections. In combination with calculations that describe cancellation of higher order corrections in asymmetries, the Q^2 dependence of the cross section may provide a complete picture of the factorization mechanism.

It has been suggested that additional information about QCD factorization may be obtained through the interference terms [29]. However, the small size of these components may complicate a definite interpretation of the experimentally fitted scaling power. A fit to the interference terms from reference [30] suggests that the Q^2-dependence is reasonably well described by a functional form $1/Q$ (χ^2=0.94, probability=0.62) for σ_{LT}/σ_L, while a functional form of $1/Q^2$ (χ^2=1.34, probability=0.51) does a reasonable job describing the Q^2-dependence of σ_{TT}/σ_L at x_B=0.311. The proposed measurement will provide access to the separated interference terms and will allow for further tests at higher values of Q^2 and x_B.

IV. PROPOSED KINEMATICS

In this experiment we propose to make coincidence measurements between charged pions in the SHMS and electrons in the HMS. The SHMS will detect pions close to the direction of $\vec{q}$ (parallel kinematics). These events correspond to θ_π near zero degrees. A high luminosity spectrometer system like the SHMS+HMS combination in Hall C is well suited for such a measurement. The magnetic spectrometers benefit from relatively small point-to-point uncertainties, which are crucial for meaningful L-T separations. In particular, the optics properties and the acceptance of the HMS have been studied extensively and are well understood in the kinematic range between 0.5 and 5 GeV, as evidenced by more than 200 L/T separations ($\sim$ 1000 kinematics) [31]. The position of the elastic peak has been shown to be stable to better than 1 MeV, and the precision rail system and rigid pivot connection allowed for reproducible spectrometer pointing for more than six years. The main properties of the HMS have been copied into the design of the SHMS, and measurements are expected to benefit from relatively small point-to-point uncertainties. Previous pion production coincidence experiments have achieved point-to-point uncertainties of $\sim$ 2%. In comparison to these experiments, which used the SOS for electron detection and the HMS for π^+ detection, we expect an additional improvement in the systematic uncertainty.

A large acceptance device like CLAS12 is well suited for measuring pseudoscalar meson electroproduction over a large range of $-t$ and x_B. Though the large azimuthal coverage allows to determine the interference terms well, the main constraint remains the error amplification in the extraction of longitudinal and transverse components. In addition, the rates for the proposed kinematics would decrease significantly due to the lower luminosity in Hall B. The use of the SHMS and HMS in Hall C is proposed here as their characteristics best address the experimental requirements, and the existing knowledge of the properties of the HMS is expected to allow for a well understood isolation of the longitudinal cross section on the order of thirty days.

Table I shows the kinematic settings proposed for this experiment. The Q^2 dependence of the cross section will be examined at several x_B points, and at fixed values of $-t$ that are small relative to Q^2. The data will be acquired in near-parallel kinematics, which will allow for the separation of the individual cross section components. We have assumed that the SHMS can be set to angles ranging between 5.5° and 30°, and that the minimum opening angle between the spectrometers can be no less than 18.0° when the HMS is located at 10.5°. To determine σ_L and σ_T from the data, a minimum of two beam energies is required. To minimize the amplification in the systematic uncertainty, the ϵ settings have been chosen to span $\Delta\epsilon \sim 0.24$ where possible. This is feasible for all but the highest Q^2 data point, where $\Delta\epsilon \sim 0.14$ is the best that can be achieved.

Figure 9 shows the accessible Q^2-x_B phase space for this experiment. The proposed kinematics allow for a scan of the Q^2 dependence of the cross section at constant x_B while staying above the resonance region. The Q^2 scans at x_B=0.31 and x_B=0.40 largely repeat the kinematics shown in Figure 6, but up to a higher value of Q^2 and in one designated measurement and hence with

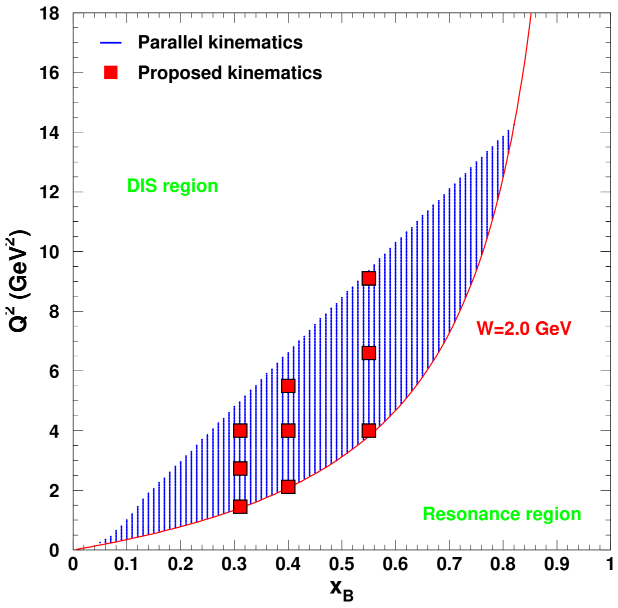

FIG. 9: *Q^2 versus x_B phase space available for L-T separations in Hall C at 11 GeV using the SHMS+HMS combination. We propose to measure the Q^2 dependence of the longitudinal cross section at x_B=0.311, 0.40 and x_B=0.55, and the x_B dependence of the longitudinal cross section at Q^2=4.0 GeV^2 (see Figure 16). The kinematic reach is limited from below by the requirement on W being above the resonance region and from above by the requirement to maintain a separation of $\Delta\epsilon \sim$ 0.24 with the exception of the highest Q^2 data point, where $\Delta\epsilon \sim$ 0.14 is the best that can be achieved.*

smaller systematic uncertainties. Since these measurements are at relatively low Q^2, these data are acquired relatively quickly and do not contribute greatly to the total beam time request. One of the goals of the proposed measurement is to extend our knowledge of the relative longitudinal and transverse contributions to the cross section to the largest possible Q^2. Given the constraint imposed by the requirement to keep $-t \ll 1$ GeV^2, combined with the maximum available beam energy of the upgraded CEBAF and the kinematic reach of the SHMS+HMS configuration in Hall C, the maximum Q^2 is near 10 GeV^2. At this point, $\Delta\epsilon$ is kinematically restricted. We have chosen to limit the maximum Q^2 to 9.1 GeV^2 as the ratio R is effectively unknown, and the projected ratio based on previous pion production data predict a rapid increase of the uncertainties between 9 and 10 GeV^2. However, it should be emphasized that the runplan requires only minor adjustments to reach a value of Q^2=10 GeV^2, should new data indicate that the uncertainties would be acceptable.

The Q^2 coverage for the proposed measurement is a factor of 3-4 larger than what one could achieve with a 6 GeV configuration [32]. This facilitates the determination of the Q^2 dependence even if the L/T ratios turn out to be less favorable than predicted by available models.

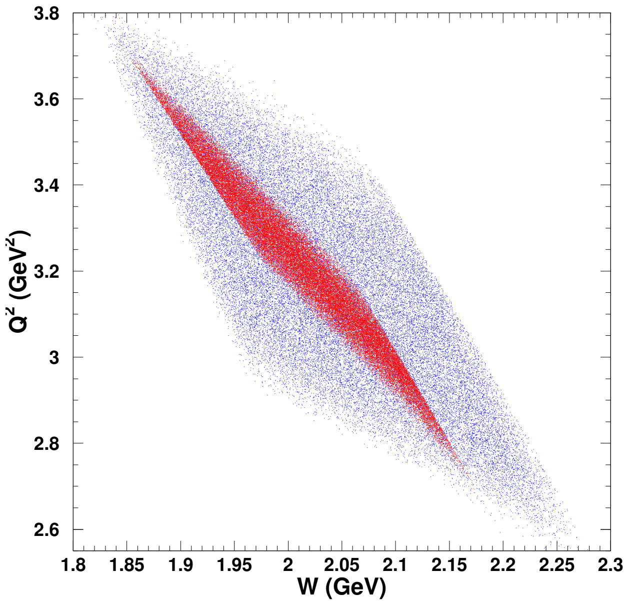

FIG. 10: *Simulated Q^2 versus W coverage for the proposed measurement at x_B = 0.40. The red data points correspond to the low and the blue data points to the high ϵ settings.*

Figure 10 shows the range of Q^2 and W acceptance at x_B=0.40. At the high ϵ setting the acceptance in W and Q^2 is generally larger than at the low ϵ point. To reduce systematic uncertainties, cuts will be placed on the data to equalize the Q^2-W coverage at high and low ϵ.

In order to examine the contribution and Q^2 dependence of the interference terms, data will also be acquired to the left and right of the $\vec{q}$. Figure 11 shows simulated x_B=0.40 SHMS+HMS data where θ_π was varied by $\pm$ 3° from the near-parallel kinematics. The ϕ coverage allows σ_{LT} and σ_{TT} to be obtained from the measured ϕ dependence of the cross section.

A. Particle Identification

The SHMS will be configured for π^+ detection and the HMS for electron detection. Hadron identification in the SHMS is primarily done with coincidence time cuts, and in-time protons and kaons are effectively eliminated. The SHMS will be equipped with a series of Cerenkov detectors to provide additional methods to distinguish pions from protons and kaons, and improve the real-to-random signal.

At hadron momenta above 3 GeV/c, time-of-flight measurements over the planned baseline for the SHMS detector stack are not reliable for separating pions and protons, and insufficient for π^+/K$^+$ discrimination. For the SHMS momenta proposed in this experiment, good π^+/K$^+$ identification can be accomplished by a C_4F_{10} heavy gas Cerenkov detector with momentum-

TABLE I: *Kinematic settings for the $p(e,e'\pi^+)$ n measurement. The scattered electron will be detected in the HMS and the π^+ in the SHMS. The proposed measurements requires three different linac energies and four pass changes. These can be achieved using two lower linac gradients of 1.82 GeV/pass, and 1.96 GeV/pass, in addition to the standard 11 GeV gradient.*

W (GeV)	Q^2 (GeV^2)	E_e (GeV)	E'_e (GeV)	θ_e (deg)	ϵ	p_π (GeV)	θ_π (deg)	$-t_{min}$ (GeV/c)^2	x	R
2.02	1.45	3.70	1.216	32.99	0.520	2.419	13.87	0.114	0.311	2.06
2.02	1.45	5.90	3.416	15.42	0.839	2.419	19.20	0.114	0.311	2.06
2.63	2.73	5.90	1.223	35.83	0.347	4.611	8.30	0.118	0.311	2.42
2.63	2.73	8.80	4.123	15.77	0.743	4.611	13.05	0.118	0.311	2.42
3.12	4.00	8.80	1.947	27.96	0.388	6.786	7.35	0.120	0.311	2.58
3.12	4.00	10.90	4.047	17.32	0.628	6.786	9.72	0.120	0.311	2.58
2.02	2.12	4.40	1.576	32.10	0.559	2.709	15.28	0.207	0.400	1.08
2.02	2.12	6.60	3.776	16.77	0.829	2.709	20.05	0.207	0.400	1.08
2.62	4.00	6.60	1.271	40.39	0.313	5.209	8.32	0.219	0.400	1.12
2.62	4.00	8.80	3.471	20.85	0.646	5.209	12.54	0.219	0.400	1.12
3.02	5.50	8.80	1.472	38.04	0.281	7.207	6.77	0.224	0.400	1.20
3.02	5.50	10.90	3.572	21.67	0.559	7.207	9.87	0.224	0.400	1.20
2.04	4.00	5.90	2.024	33.64	0.535	3.605	14.90	0.500	0.550	0.17
2.04	4.00	8.80	4.924	17.48	0.817	3.605	19.82	0.500	0.550	0.17
2.51	6.60	7.40	1.005	56.19	0.196	6.108	6.96	0.533	0.550	0.20
2.51	6.60	9.20	2.805	29.29	0.504	6.108	11.49	0.533	0.550	0.20
2.89	9.10	10.00	1.184	51.99	0.181	8.521	5.75	0.548	0.550	0.23
2.89	9.10	10.90	2.084	36.90	0.320	8.521	7.72	0.548	0.550	0.23

dependent presssure from 0.7-2.0 atm. The effect of the pressure change is to keep the optical characteristics of the Cerenkov approximately constant with momentum.

The π^+ and K$^+$ singles rates are comparable for the proposed kinematics. While kaons that propagate to the SHMS detector hut can be easily discriminated using the Cerenkov detector, a fraction of kaons produced may decay to either charged pions or muons. A significant fraction of these decay products may also propagate to the SHMS focal plane and cannot be eliminated by the Cerenkov detector. Those resulting from kaon singles events will appear as random coincidences and will be subtracted away.

Projected rates for the HMS are relatively low and are well within the operating parameters of previous HMS experiments. In this experiment we will reject π^- in the HMS at the hardware level. The electron will be identified using the lead-glass calorimeter in combination with the gas Cerenkov. On the trigger level this translates to the logical OR of the high threshold preshower and gas Cerenkov signals combined with signals from both scintillator planes. Pion rejection rates

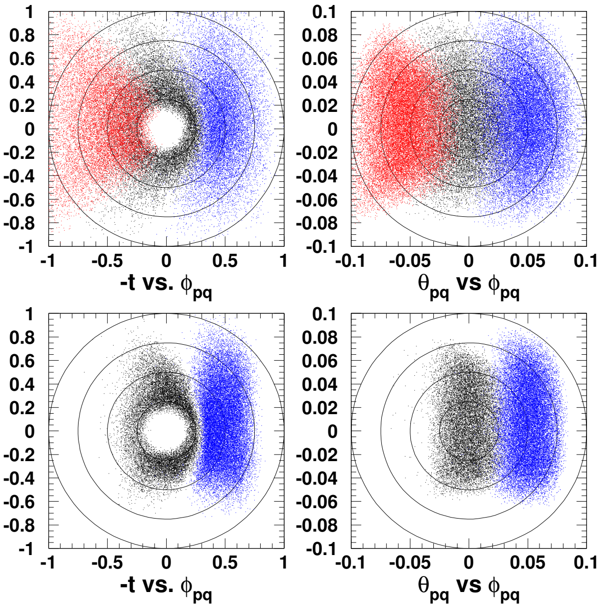

FIG. 11: *Simulated $-t$ (radial coordinate) versus the azimuthal angle ϕ distributions for the proposed measurement using HMS+SHMS at x_B=0.40 and Q^2=5.50 GeV^2. The upper two panels correspond to the high and the two lower plots correspond to the low ϵ settings. Each radial division corresponds to $-t = 0.10$ GeV^2. The colors denote the kinematic points with the SHMS set at zero (black), +2° (blue), and -2° (red).*

of 25:1 may be achieved without significant inefficiency. The trigger efficiency may be monitored using a prescaled sample of pions. Previous experiments in Hall C have shown that after offline cuts on calorimeter, Cerenkov, and coincidence time, the π^- contamination is negligible.

B. Backgrounds

Singles rates from (e, π^+) and (e, K^+) can result in accidental coincidences which are a source of background for the measurement. The singles rates into both spectrometers were estimated and are summarized in Table II. For the electron rates, the QFS program by O'Connell and Lightbody [33] was used, while the hadron rates were estimated using a fit to experimental pion and nucleon photoproduction at higher energies [34]. The projected singles rates are well below the anticipated capability of the detector packages, which we expect to be constructed to accomodate multi-MHz singles rates. At the highest Q^2 point, the K^+ singles rate is as large as 75% of the π^+ rate. However, as the SHMS heavy gas Cerenkov detector is expected to achieve better than 10^4:1 π^+/K^+ rejection ratios at 8 GeV/s [36], this is not anticipated to be a problem.

In calculating the accidental coincidence rates, the hadron trigger rate was taken to be equal to the raw trigger rate. No distinction between pions, kaons and protons was made in the trigger.

TABLE II: *Projected SHMS and HMS rates for a 8-cm LH2 target. The accidental coincidence rates assume a resolving time of 40 ns, a 25:1 π^- and K^- rejection, and correspond to the online rates. After offline cuts are applied the accidental coincidences will be effectively eliminated.*

Q^2 (GeV^2)	ϵ	R(π^+) (kHz)	R(K^+) (kHz)	R(p) (kHz)	R(π^-) (kHz)	R(K^-) (kHz)	R(e^-) (kHz)	R(acc) (Hz)	R(real) (Hz)
1.45	0.52	19.1	3.8	11.2	6.2	0.07	1.5	2.4	1.4
1.45	0.84	10.2	2.4	8.6	2.3	0.07	23.5	20.0	3.5
2.73	0.35	7.8	3.4	3.2	6.7	0.16	0.2	0.3	0.1
2.73	0.74	2.8	1.2	2.0	1.7	0.12	2.7	0.7	0.3
4.00	0.39	4.2	2.7	1.7	4.9	0.19	0.2	0.1	0.2
4.00	0.63	1.7	1.0	0.7	1.6	0.13	1.0	0.1	0.5
2.12	0.56	9.4	2.3	6.6	1.9	0.03	1.2	0.8	1.2
2.12	0.83	4.2	1.1	4.1	0.7	0.02	12.0	0.9	2.3
4.00	0.31	5.1	2.2	2.3	2.3	0.06	0.2	0.4	0.1
4.00	0.65	1.2	0.6	0.8	0.5	0.03	1.7	0.2	0.3
5.50	0.28	2.6	1.6	1.2	2.6	0.06	0.1	0.04	0.1
5.50	0.56	0.7	0.4	0.3	0.4	0.03	0.7	0.04	0.1
4.00	0.54	2.7	0.9	2.1	0.2	0.01	0.4	0.1	0.6
4.00	0.82	0.7	0.2	0.8	0.05	0.01	4.1	0.3	1.0
6.60	0.20	4.4	2.3	2.0	0.8	0.01	0.01	0.01	0.03
6.60	0.50	0.5	0.3	0.3	0.1	0.01	0.1	0.03	0.04
9.10	0.18	2.0	1.5	0.9	0.5	0.01	0.01	0.005	0.01
9.10	0.32	0.6	0.4	0.3	0.2	0.01	0.1	0.006	0.01

The online π^- rejection rate was assumed to be 25:1. The online coincidence resolving time was taken to be 40 ns. For all settings, the resulting online real+random rates are well below the expected capability of the HMS+SHMS data acquisition system. Offline, where the resolving time is expected to be no worse than 2 ns, one can see that the accidental coincidence rates are not a significant source of background. Placing cuts on the missing mass will reduce the accidental background to just a few percent of the real coincidence rate.

The unobserved exclusive final state will be identified via the missing mass, which is reconstructed from the final electron and proton four-momenta. Cutting on the missing mass will reduce both random coincidences and background from events with larger inelasticity than p$(e,e'\pi^+)$n. For example, events from the p$(e,\pi^-\pi^+)$p reaction, where the π^- is misidentified as an electron, are effectively removed. The missing mass acceptance is illustrated in Figure 12. The missing mass resolution is $\sim$ 10 MeV at the high and low Q^2 settings and should be more than adequate for separating the exclusive final state from multi-pion production.

We have chosen a liquid hydrogen target with a length of 8 cm. This means that the target

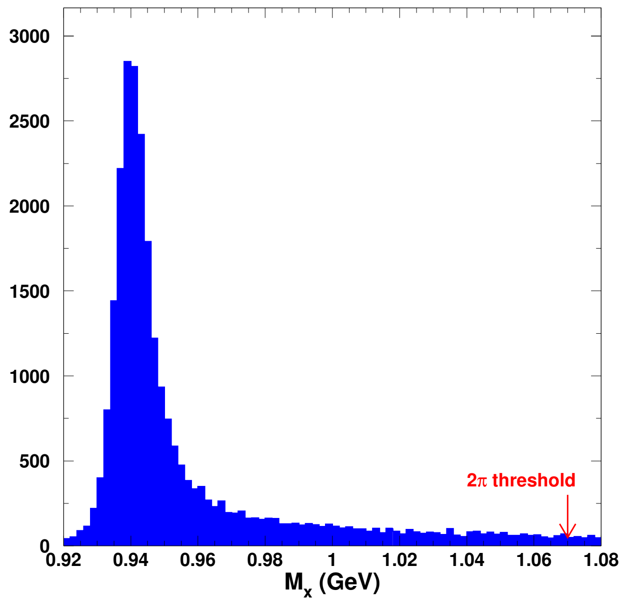

FIG. 12: *Simulated missing mass spectrum for* $Q^2 = 9.1\ GeV^2$.

end windows will be in the acceptance of both spectrometers in all configurations and background subtractions are necessary. Background events from the target end windows will be measured using "empty" target data. The Hall C empty target consists of two thin Aluminum pieces separated by a length equivalent to the cryogenic target length. However, the empty target is thicker by a factor of approximately ten relative to the target cell walls. The thicker target allows for a more rapid accumulation of counts for this background measurement. Assuming a maximum current of 30μA and 90 μA for the empty and cryo targets respectively results in a background measurement faster by a factor of 3. Based on previous measurements in Hall C [30], we estimate the surviving window background for p$(e, e'\pi^+)$n to be on the order of 1% for a 8-cm target.

C. Systematic Uncertainties

The estimated systematic uncertainties are listed in Table III. These are based on previous experience with the HMS+SOS in Hall C. Assuming that thorough sieve optics measurements are performed in the first year of SHMS operation, we expect these systematic uncertainties to be reasonably achievable. In fact, in comparison to recent coincidence measurements with the HMS+SOS we expect some improvements in the contributions to the systematic uncertainty. For example, the HMS acceptance is much flatter than the SOS acceptance and will not be affected significantly by magnetic field saturation.

Compared to previous experiments the pion momentum will be higher, and we expect the corresponding pion absorption correction to be smaller. In addition, the SHMS flight path is shorter by about a factor of two compared to the HMS. This means that the pion decay correction is smaller and the contribution to the systematic uncertainty may be scaled accordingly. In the case of π^+ detection, the SHMS performance is expected to be comparable to the systematic uncertainties characteristic for the HMS.

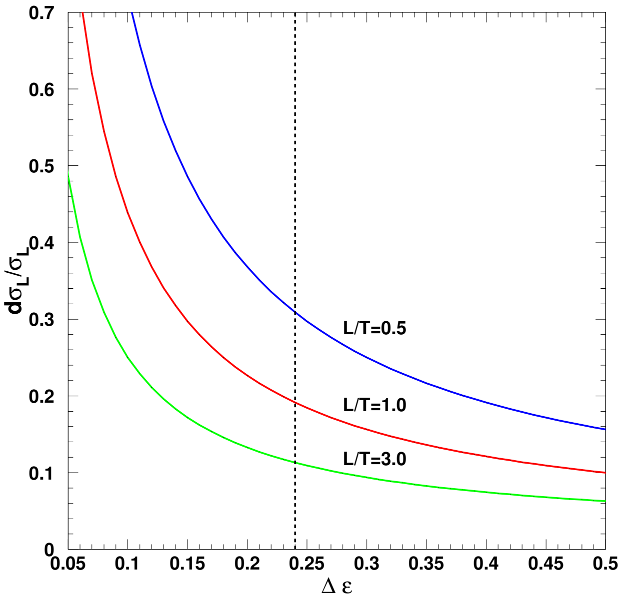

FIG. 13: *The relative uncertainty of σ_L as a function of $\Delta\epsilon$ for three values of R=σ_L/σ_T. The dominant parameter in the determination of the total uncertainty is R even if $\Delta\epsilon$ is rather small. However, the uncertainty rises nearly exponentially below $\Delta\epsilon$=0.2. The dashed line indicates the lowest value of $\Delta\epsilon$ used in the proposed measurement.*

V. PROJECTED ERROR AND TIME ESTIMATE

In preparing the count rate estimate we assume the following: 8-cm liquid hydrogen target thickness and 90 μA electron beam current, SHMS solid angle and momentum bite of 3.5 msr and 15%, and HMS solid angle and momentum bite of 5.9 msr and 8%. The dominant parameter in the beam time estimate are the ratio of longitudinal to transverse cross sections, R=σ_L/σ_T and the value of $\Delta\epsilon$ between the kinematic settings.

Two measurements at fixed Q^2 and W and different values of ϵ are required to determine σ_L. Letting $\sigma_1 = \sigma_T + \epsilon_1\sigma_L$ and $\sigma_2 = \sigma_T + \epsilon_2\sigma_L$ then

$$\sigma_L = \frac{1}{\epsilon_1 - \epsilon_2}\,(\sigma_1 - \sigma_2)\,. \qquad (7)$$

TABLE III: *Estimated systematic uncertainties for the π^+ unseparated cross section based on previous Hall C experiments. The uncorrelated errors between high and low ϵ settings are listed in the first and second column. The point-to-point uncertainties are amplified by $1/\Delta\epsilon$ in the L-T separation. The t-correlated uncertainties are also amplified, while the scale uncertainties propagate directly into the separated cross sections.*

Source	pt-to-pt	t-correlated	scale
Acceptance	0.4	0.4	1.0
PID		0.4	
Coincidence Blocking		0.2	
Tracking efficiency	0.1	0.1	1.5
Charge		0.2	0.5
Target thickness		0.2	0.8
Kinematics	0.4	1.0	
Pion Absorption		0.1	1.5
Pion Decay	0.03		0.5
Radiative Corrections	0.1	0.4	2.0
Monte Carlo Model	0.2	1.0	0.5
Total	0.6	1.6	3.3

Assuming uncorrelated errors in the measurement of σ_1 and σ_2, one obtains the intermediate expression

$$\frac{\Delta\sigma_L}{\sigma_L} = \frac{1}{\epsilon_1 - \epsilon_2}\frac{1}{\sigma_L}\sqrt{\Delta\sigma_1^2 + \Delta\sigma_2^2}, \tag{8}$$

and by defining R=σ_L/σ_T and $\Delta\sigma/\sigma = \Delta\sigma_i/\sigma_i$ and assuming $\Delta\sigma_1/\sigma 1 = \Delta\sigma_2/\sigma_2$, one obtaines

$$\frac{\Delta\sigma_L}{\sigma_L} = \frac{1}{\epsilon_1 - \epsilon_2}\frac{\Delta\sigma}{\sigma}\sqrt{(1/R + \epsilon_1)^2 + (1/R + \epsilon_2)^2}. \tag{9}$$

Equation 9 demonstrates the error amplification due to the limited ϵ range and possibly small R. For the proposed measurements $R \leq 1$. The limited ϵ lever arm is the secondary source of error amplification. However, kinematic settings with larger values of $\Delta\epsilon$ are not possible with the SHMS+HMS combination. The total uncorrelated errors between high and low ϵ settings, which are dominated by kinematic and cross section model uncertainties, are listed in Table III. Given the significant error amplification for uncorrelated errors, the correlated systematic errors of a few percent can effectively be ignored. The last column in Table III lists the correlated systematic errors.

The absolute size of the ratio of longitudinal and transverse cross sections is not well known above the resonance region and the theoretical uncertainty in the magnitude of σ_T ranges between a factor of 3-5. The longitudinal cross section predicted by the VGL/Regge model for Q^2= 4.0 GeV^2 is on the order of 0.3 μb/GeV^2 at x_B=0.55, resulting in L/T ratios of $\approx$1.2. This ratio becomes

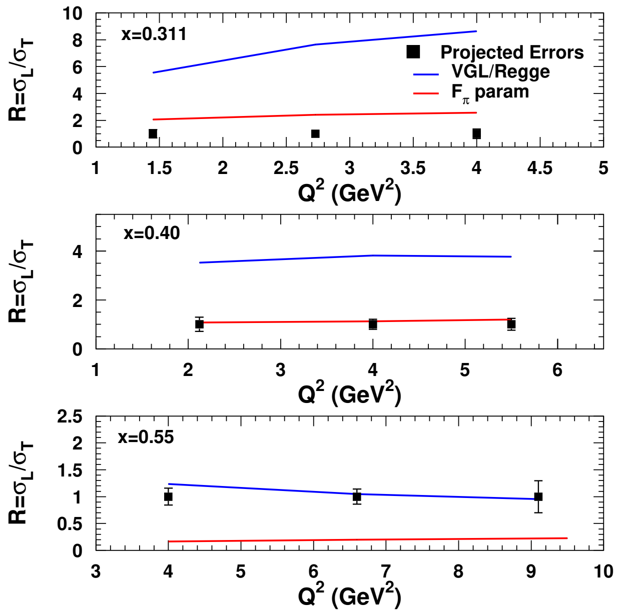

FIG. 14: *The ratio of longitudinal and transverse cross sections, R=σ_L/σ_T, as calculated using the VGL/Regge model (blue solid) and the parameterization used in this proposal (red solid). The error bars denote the uncertainty using a value for R as predicted by our parameterization. The VGL Regge model underpredicts σ_T at low Q^2 and W, but it is expected that the prediction becomes increasingly more accurate at larger Q^2 and W. Nevertheless, our parameterization conservatively assumes that the Regge calculation still underpredicts the transverse cross section even at the highest Q^2 point. Note that the proposed Q^2 points (filled symbols) were placed arbitrarily at unity.*

TABLE IV: *The projected uncertainty in the fitting exponent in the Q^n dependence.*

x_B	dn
0.31	0.3
0.40	0.4
0.50	2.0

even smaller as x_B increases, making Rosenbluth separations difficult due to the unfavorable error propagation. Predictions based on a parameterization based on previous pion production data predict a transverse cross section larger by a factor of $\sim$ 4, which gives a L/T ratio of $\approx$0.2. Recent separated cross section data from Hall C may hint that transverse contributions are indeed larger than anticipated in the VGL model or other available models.

For the rate estimate we chose to estimate the size of the longitudinal to transverse ratio from a parameterization of previous pion production data. This parameterization includes a fit to recent F_π data and the longitudinal cross section was matched to the VGL Regge prediction

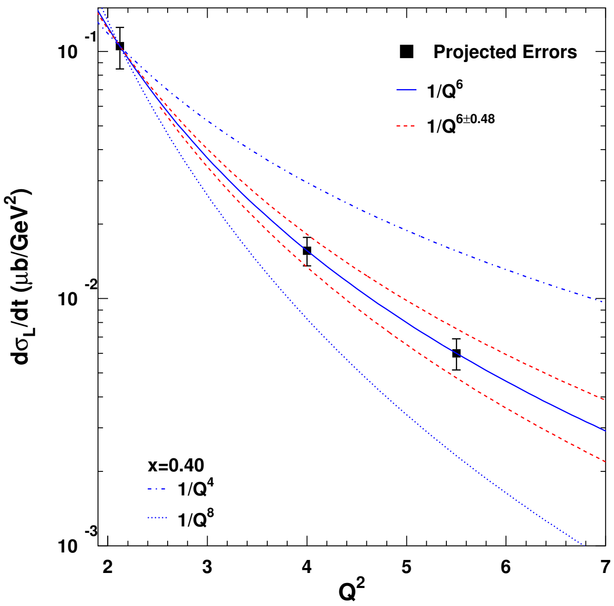

FIG. 15: *Projected uncertainties for the Q^2 dependence of σ_L at x_B=0.40. The data points are plotted to follow $1/Q^6$ scaling. The uncertainties were determined using a two parameter fit of the form A/Q^n. The red dashed curves assume a form $1/Q^n$ for the Q^2 dependence of the longitudinal cross section, and indicates the precision with which one may fit the exponent. The projected sensitivity for fitting the Q^2 dependence at x_B=0.40 and 0.55 is dn=±0.48 and dn=±2. The projected uncertainty on dn depends on the projected uncertainty for σ_L, which in turn depends on R=σ_L/σ_T. For consistency with the existing data we have used R values predicted from our parameterization. If new data suggests that the VGL prediction is more applicable at higher Q^2, this would reduce the uncertainties on dn to dn=±0.2 and dn=±1 respectively.*

at moderate and higher values of Q^2. The parameterization does a relatively good job describing the recent separated Hall C data as illustrated in Figure 6. For our kinematics, the cross section ratio as predicted by the F_π parameterization varies between 0.2 and 2.6 for values of $\Delta\epsilon$ ranging between 0.24 and 0.39 where possible. As illustrated in Figure 14, the transverse contribution as predicted by the VGL Regge calculation is significantly lower. Thus, the σ_T results of the proposed measurement will not only provide essential information on the applicability of the GPD picture at 12 GeV energies, but can also provide important information on the missing elements in the available calculations. These data may also help to constrain longitudinal backgrounds in the extraction of the pion form factor.

To illustrate the sensitivity of the experiment, the projected uncertainties the Q^2 dependence of the π^+ longitudinal cross section is shown in Figure 15. The x_B dependence is shown in Figure 16. The filled symbols indicate the proposed π^+ measurement. We assume 5,000 good events at the

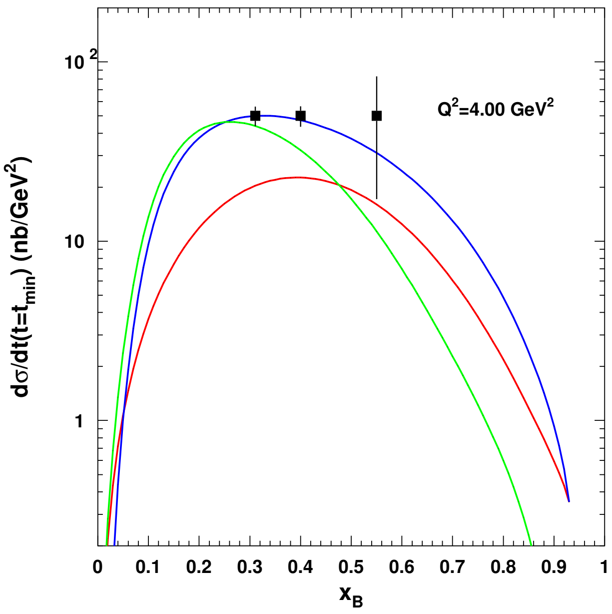

FIG. 16: *Projected uncertainties for the x_B dependence of σ_L. The proposed x_B points were placed arbitrarily at 50 nb/GeV^2.*

x_B=0.31 and x_B=0.40, and 10,000 good events at x_B=0.55 for each ϵ setting to determine the Q^2 dependence of the reaction. The uncertainties on the proposed points have been estimated using the F_π parameterization for both longitudinal and transverse cross sections, assuming a systematic uncertainty of 1.7% in the unseparated cross section, and correlated uncertainties as listed in Table III. The projected uncertainty in the fitting exponent in the Q^n dependence are listed in table IV. It should be emphasized that the projected uncertainty on dn depends on the projected uncertainty for σ_L, which in turn depends on the value of R=σ_L/σ_T. For consistency with the existing data we have used R values predicted from our parameterization. If new data suggests that the VGL prediction is more applicable at higher Q^2, this would reduce the uncertainty on dn to dn=±0.1, 0.2 and dn=±1 respectively. One can see that it is feasible to accurately determine the Q^2 dependence with the proposed measurement.

Figure 16 illustrates that the proposed measurement can relatively easily distinguish between pole and axial contributions within the framework of the GPD calculation by Vanderhaeghen, Guidal and Guichon [11].

The resulting beam time estimate is listed in Table V. Note that the projected final uncertainties depend strongly on the ratio of longitudinal to transverse cross sections. The L-T ratios assumed in the estimate are listed in Table I. These are significantly smaller than those predicted by the VGL Regge model. We thus expect that it is realistic to achieve the projected uncertainties in this experiment.

TABLE V: *Beam time estimates for the $p(e, e'\pi^+)\,n$ measurement assuming 90 μA on a 8-cm LH2 target. The projected number of hours includes three θ_π settings at high ϵ and two θ_π settings at low ϵ.*

Q^2 (GeV^2)	x_B	ϵ	LH_2 hours	Dummy hours	Overhead (hours)	Total (hours)
1.45	0.311	0.52	1.0	0.1	4	5.1
1.45	0.311	0.84	0.4	0.1	4	4.5
2.73	0.311	0.35	5.3	0.4	4	9.7
2.73	0.311	0.74	2.0	0.2	4	6.2
4.00	0.311	0.33	5.9	0.4	4	10.3
4.00	0.311	0.63	3.1	0.2	4	7.3
Subtotal x_B=0.311						43.1 (1.8 days)
2.12	0.40	0.56	1.2	0.1	4	5.3
2.12	0.40	0.83	0.6	0.1	4	4.7
4.00	0.40	0.32	11.5	0.8	4	16.3
4.00	0.40	0.72	6.0	0.4	4	10.4
5.50	0.40	0.28	21.2	1.5	4	26.7
5.50	0.40	0.56	13.5	1.0	4	18.5
Subtotal x_B=0.40						81.9 (3.4 days)
4.00	0.55	0.32	4.6	0.3	4	8.9
4.00	0.55	0.73	2.8	0.2	4	7.0
6.60	0.55	0.15	101.7	7.1	4	112.8
6.60	0.55	0.55	62.4	4.4	4	70.8
9.10	0.55	0.18	241.7	16.9	4	262.6
9.10	0.55	0.44	220.7	15.5	4	240.2
Subtotal x_B=0.50						702.3 (29.3 days)
Subtotals			705.6	49.7	72	827.3
LD2						72.0
Calibrations						48.0
beam energy changes						48.0
Total						995.3 (41.5 days)

To investigate the σ_L/σ_T ratio in π^- production on the neutron as discussed in section II D, we will repeat the x_B=0.4 setting shown in Table V with a LD2 target, using the SHMS spectrometer for both pion polarities. This additional measurement adds three days to the requested beam time. If the measurement is successful, the results can serve as a basis for a future proposal.

Our total time request is for 37.5 days of data, but additional time ($\approx$ 4 days) will be needed for calibration purposes and beam energy changes. Configuration changes have already been included in the time estimate in Table V. For example:

- $H(e,e')$p elastic data and normalization checks $\approx$ 16 hours
- Spectrometer calibrations $\approx$ 16 hours
- Optics calibrations requiring $\approx$ 16 hours
- Energy and pass changes $\approx$ 48 hours

The experiment will require three different linac energies and eight pass changes. We assume an additional 8 hours overhead for each linac energy change and 4 hours for each pass change. The experiment will make use of the SHMS+HMS spectrometers in Hall C and require a (non-standard) 8-cm cryogenic hydrogen target. That target will also be used for the approved F_π 12 GeV experiment.

VI. SUMMARY

In summary, we propose to measure the p(e,e',π^+)n reaction at fixed values of x_B=0.31, 0.40, and 0.50 and $-t$ from which the contribution due to longitudinally and transversely polarized photons will be isolated unambiguously. The momentum transferred to the electron will be as large as Q^2=9 GeV^2, the highest Q^2 for any L/T separation in pion electroproduction. The measurement will constrain the values of Q^2 for which one can reliably apply perturbative QCD concepts and extract Generalized Parton Distributions, which may influence the accessible kinematics for 12 GeV GPD studies. The measured transverse cross section will provide important information for the interpretation of existing and future Hall B data, and may help identifying possible missing elements in existing calculations. The experimental method has been successfully used in previous measurements in Hall C. Due to the anticipated characteristics of the spectrometers and detector packages, the proposed SHMS+HMS spectrometer system is well suited for the proposed measurements.

[1] T. Horn et. al., Phys. Rev. Lett **97** 192001 (2006).

[2] J.C. Collins, L. Frankfurt and M. Strikman, Phys. Rev. **D56**, 2982 (1997).

[3] L. Frankfurt, P.V. Pobylitsa, V. Polyakov and M. Strikman, Phys. Rev. **D60**, 014010 (1999).

[4] A. Radyushkin, hep-ph/0101225, (2001).

[5] K. Goeke, V. Polyakov and M. Vanderhaeghen, Prog. Part. Nucl. Phys. **47**, 401 (2001).

[6] L. Mankiewicz, G. Piller and A. Radyushkin, Eur. Phys. J. **C10**, 307-312 (1999).

[7] M. Vanderhaeghen, P.A.M Guichon, and M. Guidal, Phys. Rev. Lett. **80**, 5064 (1998).

[8] Y. Roblin and F. Sabatie, Deeply Virtual Compton Scattering at 6 GeV, proposal to Jefferson Lab PAC18.

[9] C. Munoz Camacho et al., Phys. Rev. Lett. **97**, 262002 (2006).

[10] L. Elouadrhiri, A. Biselli, S. Niccolai, K. Joo, Deeply Virtual Compton Scattering at 6 GeV with polarized target and polarized beam using the CLAS detector, proposal to Jefferson Lab PAC 28.

[11] M. Vanderhaeghen, P.A.M Guichon, and M. Guidal, Phys. Rev. **D60**, 094017 (1999).

[12] G. Huber and D. Gaskell, Measurement of the Charged Pion Form Factor to High Q^2, JLab 12 GeV Proposal PR12-06-101, 2006.

[13] M. Vanderhaeghen, M. Guidal and J.-M. Laget, Phys. Rev. **C57**, 1454 (1998); Nucl. Phys. **A627** 645 (1997).

[14] T. Horn et. al., Scaling study of the pion electroproduction cross sections and the pion form factor (2007).

[15] H. Avagyan, private communication (2006).

[16] J.M. Laget, private communication (2007).

[17] A.V. Raduyshkin, Phys. Lett. **B642**, 459-468 (2006).

[18] M. Garcon, M. Guidal, E. Smith, Deeply Virtual Electroproduction of Vector Mesons, TJNAF Proposal e99-105 (1999).

[19] J. Volmer et al., Phys. Rev. Lett., **86**, 1713 (2001).

[20] V. Tadevosyan et al., nucl-ex/0607007 (2006).

[21] D. Gaskell et al., Phys. Rev. Lett. **87**, 202301 (2001).

[22] D. Dutta, R. Ent, K. Garrow, Measurement of Pion Transparency in Nuclei, TJNAF Proposal 01-107, 2001.

[23] C. Hadjidakis et al., Phys.Lett. **B605** 256-264 (2005).

[24] L. Morand et al., Eur.Phys.J.**A24**, 445-458 (2005).

[25] Transverse Polarization Effects in Hard Scattering at CLAS, letter of intent to Jefferson Lab PAC 30 (2006).

[26] I.T. Obukhovsky, private communication (2007); arXiv:0706.1844v1 (2007).

[27] D. Gaskell, Ph.D. thesis, Oregon State University (2001).

[28] A.V. Belitsky and D. Mueller, Phys. Lett. **B513**, 349-360 (2001) [hep-ph/0105046].

[29] K. Joo, M. Ungaro, C. Weiss, V. Kubarovsky and P. Stoler, Hard Exclusive Electroproduction of π^0 and η with CLAS12, JLab 12 GeV Proposal PR12-06-101, 2006.

[30] T. Horn, Ph.D. thesis, University of Maryland (2006).

[31] M.E. Christy et al., Phys. Rev. **C70** 014206 (2004).

[32] D. Gaskell, D. Mack, A Search for Evidence of Soft-Hard Factorization in Charged Pion Electroproduction, TJNAF Proposal (2003).

[33] J. O'Connell and J. Lightbody, Comp. in Phys., May-June **57**, (1998).

[34] wiser.f by Steve Rock, Wiser fit of proton, pion and kaon cross sections.

[35] SIMC: Monte Carlo for Hall C, (2001).

[36] G. Huber, SHMS Heavy Gas Cerenkov Detector Design, April 1, (2002).